

Shaking table test and numerical simulation of a 1/2-scale self-centering reinforced concrete frame

Xilin Lu^{1,*†}, Ye Cui¹, Jingjing Liu^{1,2} and Wenjun Gao¹

¹State Key Laboratory of Disaster Reduction in Civil Engineering, Tongji University, Shanghai 200092, China

²Faculty of Forestry, University of British Columbia, Vancouver V6T 1Z4, Canada

SUMMARY

Self-centering reinforced concrete frames are developed as an alternative of traditional seismic force-resisting systems with better seismic performance and re-centering capability. This paper presents an experimental and computational study on the seismic performance of self-centering reinforced concrete frames. A 1/2-scale model of a two-story self-centering reinforced concrete frame model was designed and tested on the shaking table in State Key Laboratory of Disaster Reduction in Civil Engineering at Tongji University to evaluate the seismic behavior of the structure. A structural analysis model, including detailed modeling of beam–column joints, column–base joints, and prestressed tendons, was constructed in the nonlinear dynamic modeling software OpenSEES. Agreements between test results and numerical solutions indicate that the designed reinforced concrete frame has satisfactory seismic performance and self-centering capacity subjected to earthquakes; the self-centering structures can undergo large rocking with minor residual displacement after the earthquake excitations; the proposed analysis procedure can be applied in simulating the seismic performance of self-centering reinforced concrete frames. To achieve a more comprehensive evaluation on the performance of self-centering structures, research on energy dissipation devices in the system is expected. Copyright © 2015 John Wiley & Sons, Ltd.

Received 13 January 2014; Revised 5 January 2015; Accepted 9 January 2015

KEY WORDS: self-centering system; reinforced concrete frame; shaking table test; numerical model

1. INTRODUCTION

1.1. Background

As a current state-of-the-art branch of the structural design to resist seismic loading, earthquake-resilient structures have gained widespread concern in both academia and industry during the past few decades. This innovative system can not only protect life safety by preventing structural failure in an earthquake but also restore its structural function immediately afterwards [1]. There are generally at least three kinds of earthquake resilient systems, including replaceable members, self-centering structures, and rocking systems. Previous research indicates that rocking of structures lowers the seismic excitation and ductility requirement of the structures. Relaxing the constraints between components or structure and base, the interfaces in the joints can undergo compression but no tension. Post-tensioned (PT) prestressed tendons can provide the forces for self-centering when the structure rocks under the earthquake [2]. A controlled rocking occurs at the beam–column joint, or the column–base joint, characterized by the so-called flag-shaped hysteretic behavior displayed in Figure 1. Controlling residual deformation of structures effectively can lead to less repair time and cost.

The concept of ‘self-centering’ was first put forward by Priestley in ‘Overview of PRESSS research program’ [3]. Priestley and Tao [4] conceived the idea of connecting precast concrete beam and

*Correspondence to: Xilin Lu, State Key Laboratory of Disaster Reduction in Civil Engineering, Tongji University, Shanghai 200092, China.

†E-mail: lxlst@tongji.edu.cn

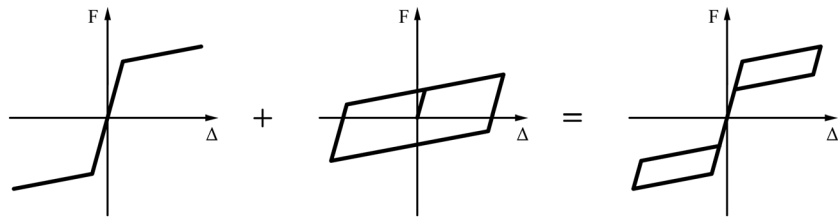


Figure 1. ‘Flag-shaped’ hysteresis behavior.

column with prestressed tendons. The tendons were debonded in the joints and at the end of the beams. Cheok and Lew [5] carried out a series of tests of precast concrete beam-to-column connections subject to cyclic loading. Seismic testing of precast beam-to-column joint subassemblies with unbonded tendons were conducted by Priestley and Macrae [6]. Priestley *et al.* [7] conducted a test of a large-scale five-story precast concrete building. Studies of numerical simulation of self-centering members and structures were carried out accordingly. By using nonlinear push-over static analyses and time-history dynamic analyses, El-Sheikh *et al.* [8] studied the behavior of two 6-story unbonded PT precast concrete frames. Spieth *et al.* [9] developed a modeling approach to model PT precast reinforced concrete frame structures with rocking beam–column connections, which gave an accurate simulation of the developed compression zone and the shift of the neutral axis in the contact area during the earthquake. Roh and Reinhorn [10] provided a simplified analytical model and computational tools for rocking columns. Hawileh *et al.* [11] constructed a detailed three-dimensional nonlinear finite element model to study the response and predict the behavior of precast hybrid beam–column connection subjected to cyclic loads. During the last decade, several research on self-centering steel frame structures were also conducted. Rojas *et al.* [12] and Garlock *et al.* [13] developed PT steel moment-resisting frames with friction devices or angle steel connections. Midorikawa *et al.* [14] carried out three-dimensional shaking table tests on seismic response of reduced-scale steel rocking frames. Ma *et al.* [15] did a series of large-scale shaking table tests of steel braced frame with controlled rocking and energy dissipating fuses.

It is noted that previous research has been focusing on self-centering members or steel frame structures. With few studies on the whole self-centering structures, especially for reinforced concrete ones, the shaking table test and numerical simulation of the designed self-centering reinforced concrete frame presented in this paper will fill the gaps in the literature and lead to a better understanding of self-centering structures.

1.2. Scope

A 1/2-scale model of a self-centering reinforced concrete frame with two-story based on a one-bay one-span prototype was adopted in this study. It was designed and tested on the shaking table in State Key Laboratory of Disaster Reduction in Civil Engineering at Tongji University as the first shaking table test of large-scale self-centering reinforced concrete structures in China. The dynamic characteristics of the structure as well as the dynamic response and damage under different levels of earthquakes were investigated. Detailed models of beam–column joints, column–base joints and prestressed tendons were presented. A computational numerical model was developed and validated through the experimental data. The results were discussed to evaluate the seismic performance of self-centering reinforced concrete structures.

2. EXPERIMENTAL SETUP AND PROCEDURE

2.1. Description of the prototype and test model

The prototype building is a two-story reinforced concrete frame, designed and detailed according to Chinese Code for design of concrete structures [16]. The dimensions of the buildings are 6.0 m × 3.0 m with one bay in both of the X and Y directions (Figure 2). The self-centering frame is

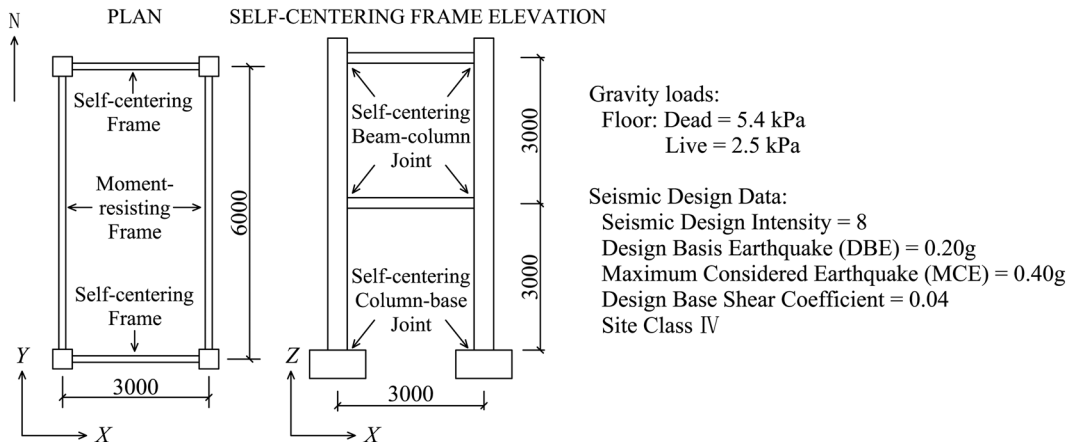


Figure 2. Prototype building design (unit: mm).

only used in the X direction for lateral resistance. Gravity loads and seismic design data are also detailed in Figure 2.

On the basis of the prototype design, the self-centering reinforced concrete frame was scaled to a 1/2-scale model to meet the physical limitations of the shaking table. The model was designed and fabricated under the similitude law [17]. Table I shows the similitude scale factor of the model. Self-centering joints, including column–base joints and beam–column joints, were specially designed, detailed in Section 2.2. Materials were selected on the basis of the mechanical property similarities between test model and the prototype. The parameters of fine aggregate concrete and reinforcement were shown in Table II. A rigid concrete block was applied to each floor, bolted to the non-self-centering beams, representing the floor slab and added mass. Two steel beams were hinged to the main beams to support the block above at each floor. The total weight of the structure was 13.0 t, whereas the added mass was 4.8 t each. Figure 3 shows the configuration of the model.

2.2. Self-centering design for the model

Figure 4(a) shows the details of column–base joints. Columns were fastened in the base pits by prestressed tendons. The prestressed tendons were pre-placed in the columns. The bottom ends of the tendons were anchored in the base pits before casting concrete, and the other ends were prestressed on the top of columns before testing. The longitudinal bars were welded to the steel plates at the bottom of the columns. The interfaces between the steel plates at the bottom of the columns and those in the base were separated to assure possible uplift for the columns under design excitation, which was El Centro 0.2 g (g is the acceleration due to gravity). Rubber was placed in

Table I. Similitude scale factors.

Parameter	Relationship	Model/prototype
Length	S_l	0.500
Young's modulus	S_E	1.000
Stress	$S_\sigma = S_E$	1.000
Strain	S_σ / S_E	1.000
Density	$S_\sigma / (S_a \cdot S_l)$	2.000
Force	$S_\sigma \cdot S_l^2$	0.250
Mass	$S_p \cdot S_l^3$	0.250
Rigidity	$S_E \cdot S_l$	0.500
Time	$(S_m/S_k)^{1/2}$	0.707
Frequency	$1/S_t$	1.414
Velocity	S_l/S_t	0.707
Acceleration	S_a	1.000

Table II. Parameters of concrete and reinforcement.

Material	Type	Cube compressive strength $f_{cu,k}$ (MPa)	Yield strength f_y (MPa)	Tensile strength f_u (MPa)	Young's modulus (MPa)
Concrete	C40 (first floor)	40.3	—	—	3.24×10^4
	C40 (second floor)	50.9	—	—	4.13×10^4
Reinforcement	HPB 235	—	235	310	2.1×10^5
	HRB 335	—	335	510	2.1×10^5

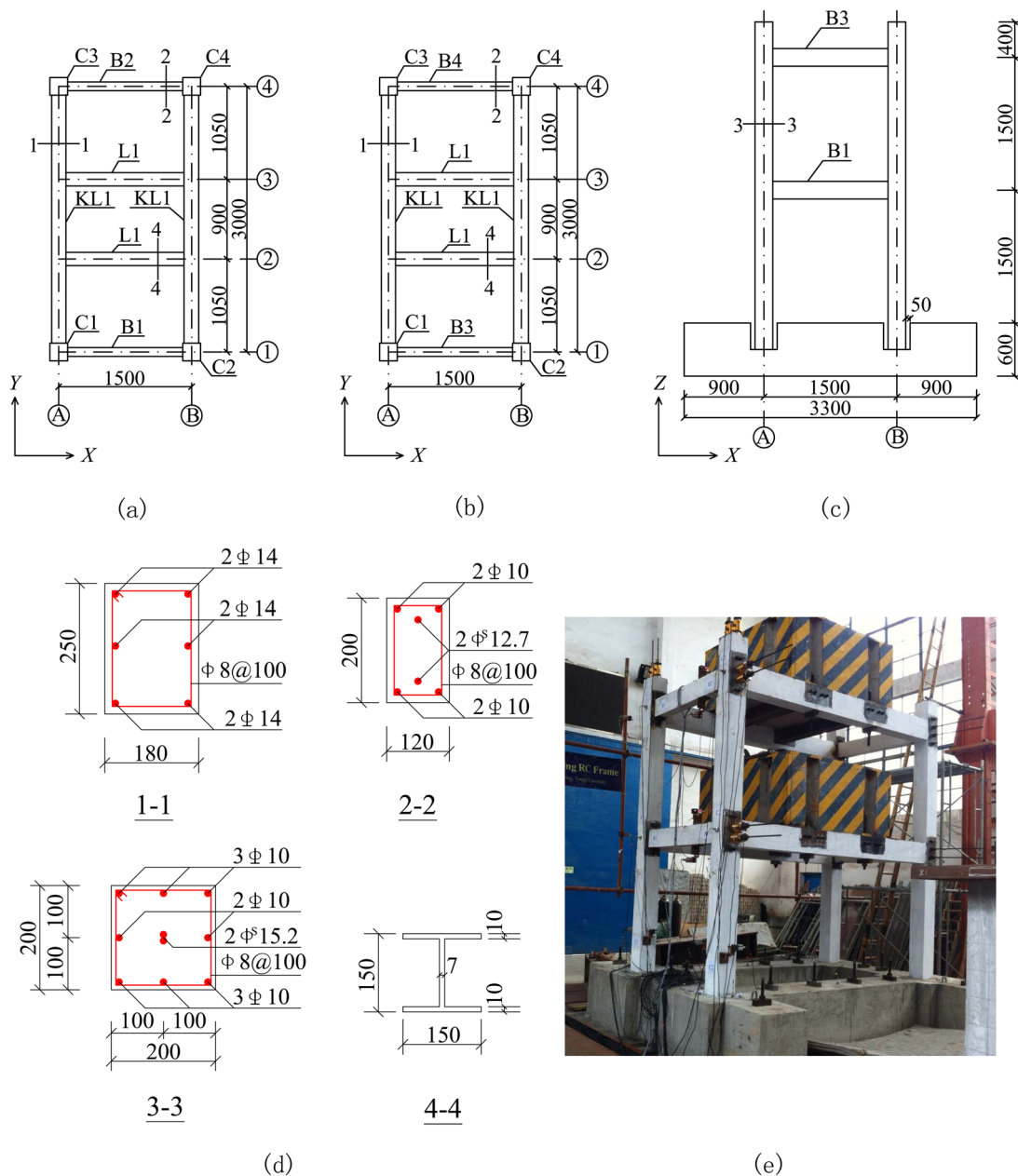


Figure 3. Configuration of frame model (unit: mm): (a) plan of the first floor, (b) plan of the second floor, (c) elevation, (d) cross section and reinforcement details, and (e) photo of the test model.

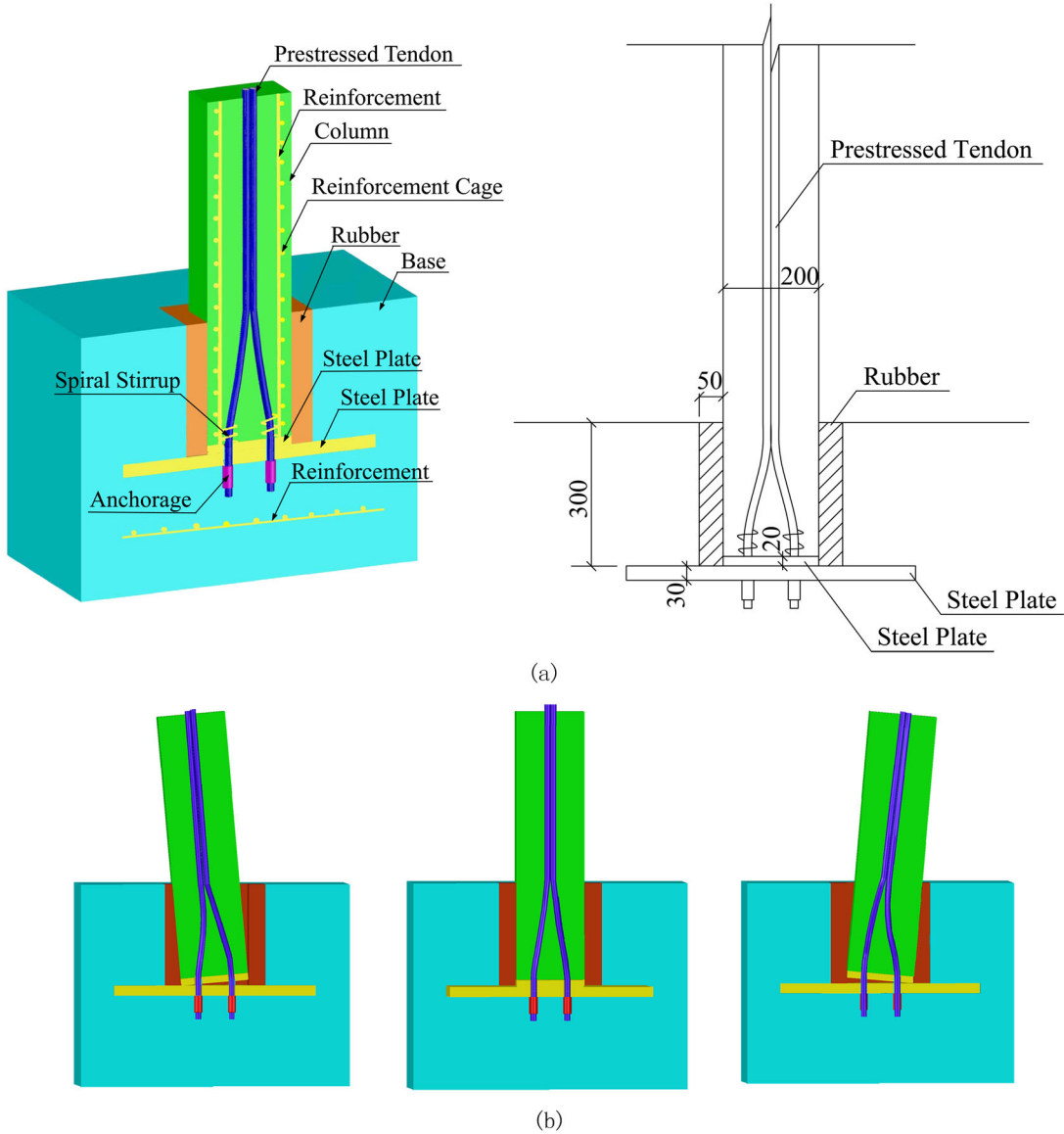


Figure 4. Column–base joint: (a) details and (b) opening.

the interspace between columns and the base to prevent the local failures of concrete. In the rocking phase, the stiffness of the structure is controlled by the stiffness of the rubber blocks. The rubber block should be thin enough to provide sufficient stiffness so that the whole structure will demonstrate positive stiffness in all designed status. Meanwhile, the rubber should be thick enough to provide adequate deformation space and prevent both column and the base from local damage so that the column can undergo large deformation (which is recorded 4.0% maximum story drift in the experiment). Therefore, the thickness of the rubber blocks is selected as 50 mm. Figure 4(b) shows the opening mechanism of the joints under earthquake excitations.

On the basis of the design excitation, the minimum opening moment of the column–base joints can be obtained. The parameters of prestressed tendons in columns can be selected accordingly (shown in Table III). Table IV shows the parameters of the rubber.

Figure 5 presents the details of beam–column joints in the self-centering frames. Beams and columns were connected by prestressed tendons. Steel plates were set at the ends of beams and the sides of columns to prevent local failures. Top and seat angle steel connections were used to enhance the shear strength and stiffness of the joints. They also worked as energy dissipation

Table III. Parameters of prestressed tendons.

Member	Size	Prestressed tendons	Yield strength		Tensile strength		Prestressed force in each tendon (kN)
			f_y (MPa)	f_u (MPa)	Young's modulus (MPa)		
Column	200 mm × 200 mm	2Φ ^s 15.2	1581.0	1860	1.95×10^5	43	
Beam	200 mm × 120 mm	2Φ ^s 12.7	1673.7	1860	1.95×10^5	43	

Table IV. Parameters of the rubber.

Material	International rubber hardness (IRHD)	Elastic modulus	Shear modulus	Thickness
Rubber	60	4.45 N/mm ²	1.06 N/mm ²	50 mm

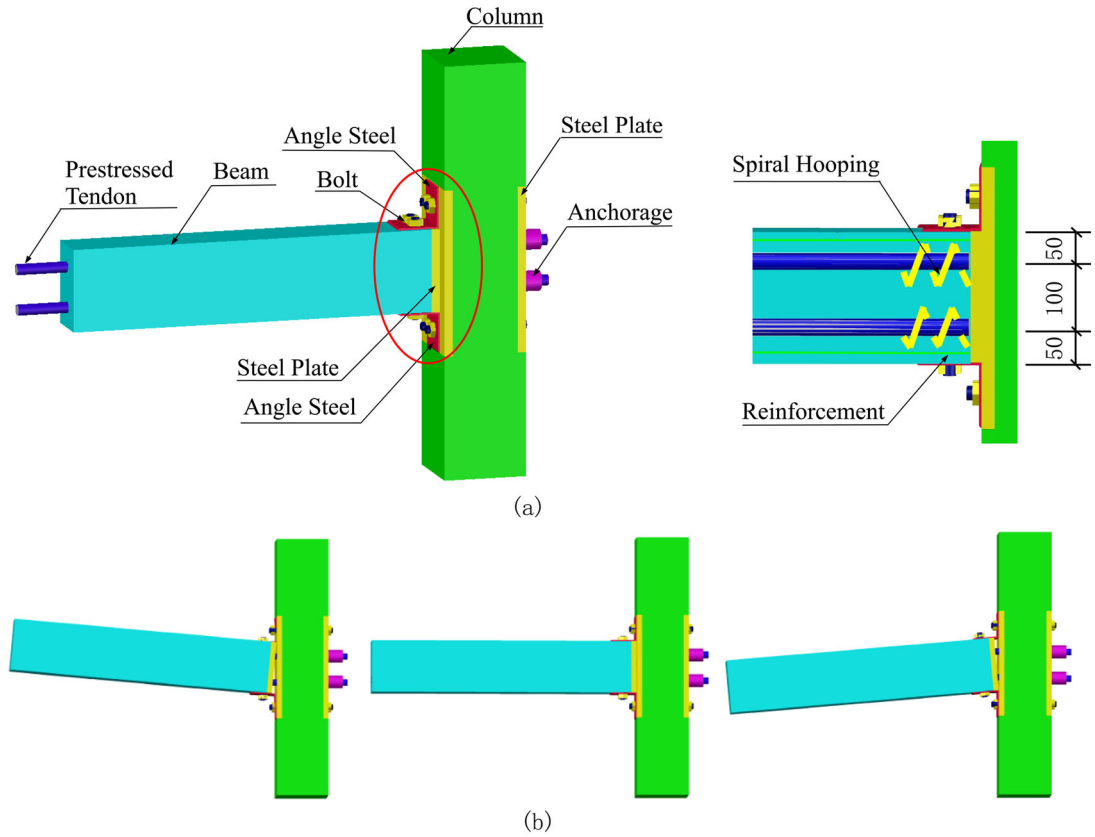


Figure 5. Beam–column joint: (a) details and (b) opening.

devices after the joints opened. The joints were expected to firstly open at the interfaces between the steel plates under design excitation (El Centro 0.2 g). Figure 5(b) shows the opening mechanism of joints under earthquake excitations.

The joints were designed using the same criteria as the column–base joints without considering the effect of the angle steel. The parameters of prestressed tendons in beams are also shown in Table III.

To ensure that the prestressed tendons remain linear elastic during the tests, it is suggested that the ultimate moment of the prestressed tendons should be larger than 1.15 times as much as that of the energy dissipation devices in New Zealand design standard for the precast reinforced concrete structures [18], and according to the design method by Yuan *et al.* [19], L100×100×4.5 angle steel

with a thickness of 4.5 mm was selected, with the yielding strength of 235 MPa. The bolt on the L100×100×4.5 angle steel was M12.

2.3. Ground motions and instrumentation

Condition of site soil is an important factor in determining the earthquake inputs for the dynamic test. Taking condition of site soil into consideration, two seismic ground motions were input to the shaking table in the test: (i) El Centro NS record from the California Imperial Valley earthquake of 18 May 1940, which is specified for the particular soil conditions of Types III and IV in China, and (ii) Wenchuan EW record from the Wenchuan earthquake of 12 May 2008, which is specified for the particular soil conditions of Types II and III in China [20]. Figure 6 shows the time history and response spectrum of the El Centro and the Wenchuan wave, respectively. It is inferred that the spectrum component of the two inputs is rich enough for the study.

Both of the ground motions were applied only in the X direction and scaled in time by a factor of 0.707 as described in Section 2.1. The ground motions were increased at increments of peak ground acceleration (PGA) by 0.05 g starting from 0.05 g. The maximum level test was the El Centro 0.60 g test and the Wenchuan 0.80 g test. The uplift of column–base joints and opening of beam–column joints were expected to be detected under the design basis earthquake (DBE) level test, and the test model was expected to neither collapse nor suffer damage when subjected to the maximum considered earthquake (MCE) level test. To detect changes in the natural frequencies of the structure, white noise scanning was conducted before and after each excitation. Table V lists the test program and the designed PGAs. Sequences 1 to 18 were applied in the first series and sequences 19 to 29 in the second series. There was a 2-day interval between the two series.

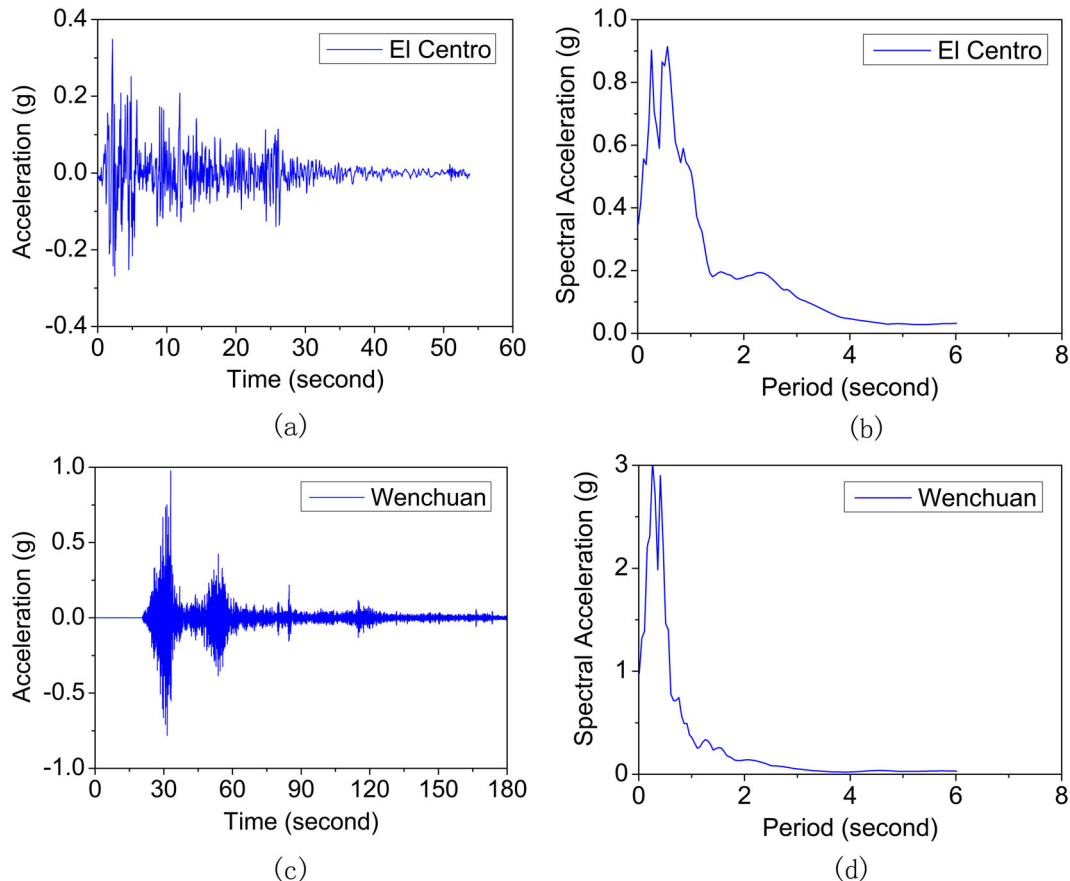


Figure 6. (a) Time history of El Centro NS, (b) response spectrum of El Centro NS (damping ratio 0.05), (c) time history of Wenchuan EW, and (d) response spectrum of Wenchuan EW (damping ratio 0.05).

Table V. Test program.

Sequence	Input	PGA (g)	Sequence	Input	PGA (g)	Sequence	Input	PGA (g)
1	WN	0.050	11	WN	0.050	21	WN	0.050
2	EL	0.050	12	EL	0.400	22	WE	0.300
3	EL	0.100	13	EL	0.450	23	WN	0.050
4	EL	0.150	14	WN	0.050	24	WE	0.400
5	WN	0.050	15	EL	0.500	25	WN	0.050
6	EL	0.200	16	WN	0.050	26	WE	0.600
7	EL	0.250	17	EL	0.600	27	WN	0.050
8	EL	0.300	18	WN	0.050	28	WE	0.800
9	WN	0.050	19	WN	0.050	29	WN	0.050
10	EL	0.350	20	WE	0.200			

WN, white noise; EL, El Centro NS; WE, Wenchuan EW.

Five kinds of sensors were used to record the response of the structural models as follows: (i) 12 linear variable differential transducers, measuring the displacement of each story of the frame; (ii) eight linear variable differential transducers, measuring the joint response to assess the opening and uplift of the joints; (iii) eight load cells, measuring the axial force of the post-tensioning tendons in the beams (B1, B3) and columns (C1, C2); (iv) eight accelerometers, measuring the horizontal and vertical acceleration at each floor; and (v) four strain gages, measuring the strain of the steel connections of the beam–column joints (the angle steel connecting B1 and C2, and B3 and C2). Figure 7 depicts the position of the sensors.

3. SYSTEM RESPONSE

3.1. Dynamic characteristics of the test model

To obtain the dynamic characteristics of the test model, white noise test was carried out. Figure 8 shows the first and second frequencies of vibration in the X direction estimated from each white noise test. The initial first mode of the test model was 4 Hz. After the tests in the first series, the first frequency fell to 2 Hz, which was 50% of the initial value. The first natural frequency rose slightly to 2.25 Hz after the 2-day interval. The first frequency fell to 1.75 Hz after the second-series tests.

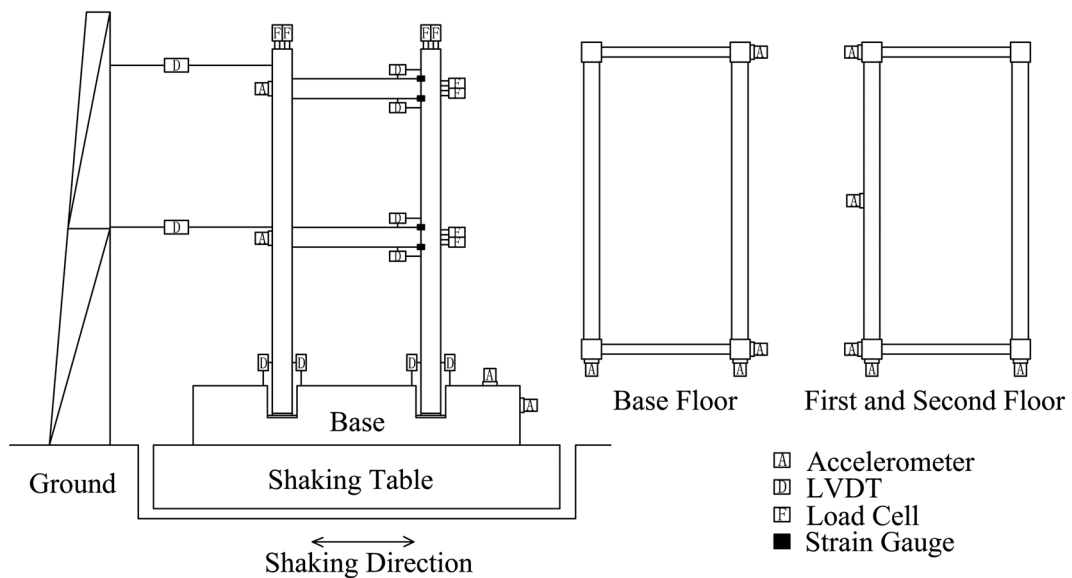


Figure 7. Sensor arrangement.

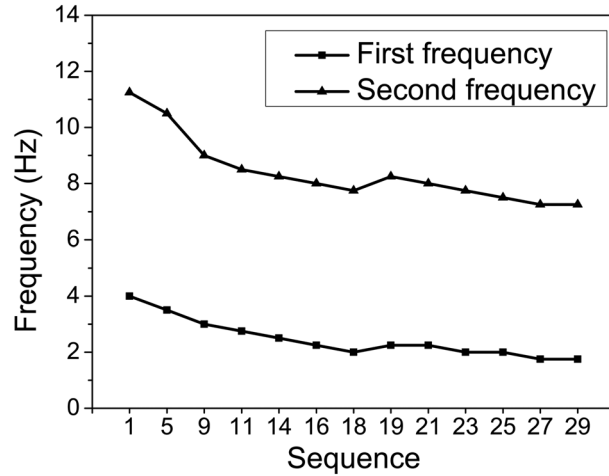


Figure 8. Changes in frequency.

This indicates the post-earthquake stiffness of the structure decreased, which was possibly due to the loss of the stress of the prestressed tendons. Tiny cracks developed on the non-self-centering beams (beams in the Y direction) when the additional masses were loaded on the test frame before the tests in the first series. Small pieces of concrete around the angle steel were crushed after the tests.

3.2. Global response

Table VI shows the maximum acceleration response and amplification factors of model acceleration (K , which is the ratio of the floor acceleration to the ground acceleration) under different earthquake excitations at each floor of the test frame. As the PGA increased, the amplification factor decreased slightly as a result of the degradation of the stiffness of the model. The amplification factors of the test model differed from each other under El Centro and Wenchuan waves.

Table VI also shows the maximum relative displacement response and residual displacement response for each test at each floor of the test frame. Figure 9 shows how the inter-story drift

Table VI. Global response.

Sequence	Input	PGA (g)	First floor				Second floor			
			a_{\max} (g)	K	X_{\max} (mm)	$X_{r,\max}$ (mm)	a_{\max} (g)	K	X_{\max} (mm)	$X_{r,\max}$ (mm)
2	El Centro	0.05	0.080	1.798	1.140	-0.182	0.104	2.358	1.342	-0.242
3		0.10	0.240	2.045	4.238	-0.007	0.305	2.602	5.965	0.024
4		0.15	0.289	1.562	4.723	0.140	0.370	1.981	7.414	0.143
6		0.20	0.523	2.116	12.035	0.121	0.649	2.628	19.801	0.189
7		0.25	0.584	2.240	17.139	0.424	0.783	3.003	28.923	0.662
8		0.30	0.722	2.479	22.216	0.465	0.757	2.600	37.055	0.747
10		0.35	0.650	1.756	31.712	0.404	0.948	2.588	55.186	0.598
12		0.40	0.768	1.835	37.232	0.511	1.077	2.573	64.993	0.921
13		0.45	0.922	1.844	45.213	0.617	1.120	2.241	78.857	1.176
15		0.50	1.283	2.113	58.517	-2.280	1.395	2.297	104.482	-3.892
17		0.60	0.853	1.386	72.649	-3.688	1.455	2.365	131.090	-6.509
20	Wenchuan	0.20	0.146	0.732	7.205	-0.076	0.206	1.034	12.708	-0.097
22		0.30	0.215	0.705	11.445	-0.164	0.345	1.127	21.559	-0.136
24		0.40	0.301	0.646	13.891	-0.158	0.415	0.892	26.659	-0.397
26		0.60	0.441	0.613	21.851	-0.069	0.562	0.780	40.634	-0.152
28		0.80	0.715	0.684	25.789	-0.088	0.639	0.612	47.168	0.010

a , acceleration response; K , amplification factor; X , relative displacement response; X_r , relative residual displacement response.

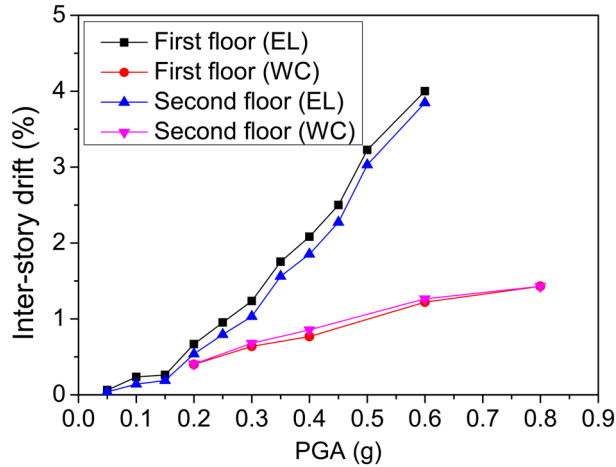


Figure 9. Changes in inter-story drift.

changes with the increase of PGA. The maximum displacement grew with the increase of PGA. There was a considerable increase of the displacement when the maximum PGA reached 0.20 g because the self-centering joints opened at this point. Under seismic loads, the maximum floor displacement was 72.649 mm at the first floor and 131.090 mm at the second floor under the El Centro 0.60 g test. Meanwhile, the inter-story drift reached 4.0% at the first floor and 3.8% at the second floor, respectively. The test frame re-centered with minimal residual displacements after the test runs because the prestressed tendons in the beams and columns remained elastic throughout the tests. Figure 10 shows the top floor displacement time history curve under the El Centro 0.60 g and Wenchuan 0.80 g tests. The residual displacements were minimal, which demonstrated the expected self-centering capability of the system. Similar to the acceleration response, the displacement response of the test model also differed a lot under different earthquake excitations.

3.3. Joint response

Table VII shows the maximum uplift of the column–base joints and opening of beam–column joints. Uplifts and openings first happened under the El Centro 0.20 g test and the Wenchuan 0.30 g test. Sounds of impact between the steel plates were heard when the maximum PGA reached 0.40 g. Under the El Centro 0.60 g test, the maximum uplift for column was 9.054 mm, and the maximum opening for beam was 9.360 mm, which were significant openings of the self-centering joints. The rocking of the column were also observed. Figure 11 shows a picture of the uplift at the base and the opening at the beam end. Figure 12 shows the column uplift time history curve and beam opening time history curve under the El Centro 0.60 g test. It can be found that the column–base

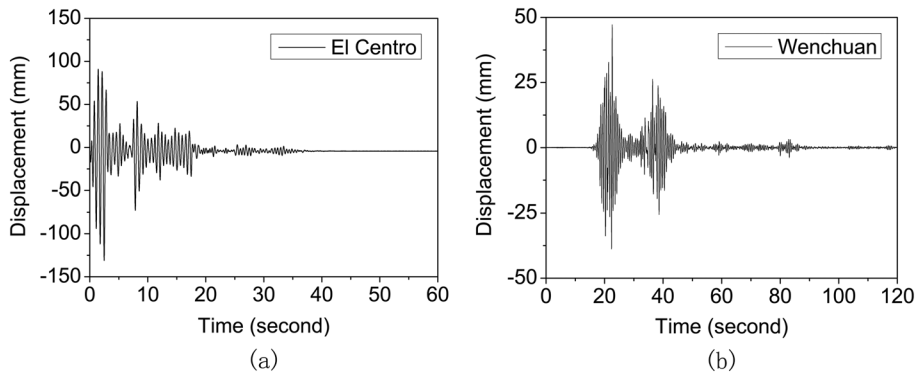


Figure 10. Top floor displacement time history curve: (a) under El Centro 0.60 g test and (b) under Wenchuan 0.80 g test.

Table VII. Joint response.

Sequence	Seismic input	PGA (g)	Maximum uplift (mm)		Maximum opening (mm)		Strain/ 10^{-6}			
			C1	C2	B1	B3	B3T	B3B	B1T	B1B
2	El Centro	0.05	0.038	0.177	0.108	0.014	24	12	10	10
3		0.10	0.362	0.377	0.283	0.127	192	63	110	157
4		0.15	0.472	0.211	0.411	0.166	267	102	111	217
6		0.20	1.164	1.317	1.285	0.827	1299	878	1112	1108
7		0.25	1.567	1.760	1.721	1.165	1725	1439	1740	1672
8		0.30	2.139	2.434	2.418	1.802	2929	2045	2534	2434
10		0.35	3.198	3.582	3.191	2.783	2861	2147	2894	3733
12		0.40	3.816	4.261	4.353	3.427	3122	2762	3233	9836
13		0.45	4.711	5.250	5.482	4.219	3716	3424	3352	2752
15		0.50	6.312	7.036	7.347	4.511	4193	4170	5767	1712
17		0.60	8.123	9.054	9.360	7.699	5505	5508	8719	1875
20	Wenchuan	0.20	0.643	0.641	0.804	0.690	169	787	740	—
22		0.30	1.146	1.094	1.400	1.345	343	1202	1015	—
24		0.40	1.375	1.269	1.794	1.768	459	1212	1130	—
26		0.60	2.216	2.027	2.812	2.570	549	1245	1147	—
28		0.80	2.479	2.384	3.218	2.994	748	1404	1352	—

B1, beam B1; B3, beam B3; T, top; B, bottom.



Figure 11. The uplift at the base and the opening at the beam end.

joints uplifted and the beam–column joints opened during the test, and the test frame re-centered after the test. The residual opening and uplift were minimal, which demonstrated the expected self-centering capability of the designed structure.

The initial stress of prestressed tendons in columns were 300 and 425 Mpa for beams. During the test, the maximum stress of prestressed tendons in columns and beams were 473.185 and

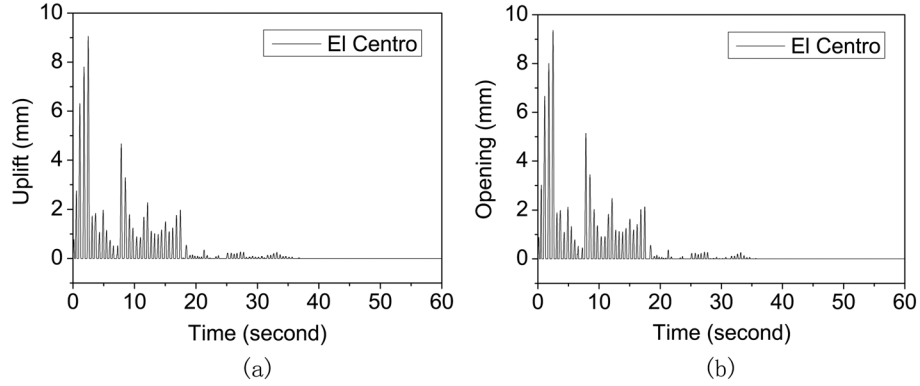


Figure 12. Time history curves of the uplift at the base and the opening at beam ends under El Centro 0.60 g:
(a) the uplift at the base and (b) the opening of beam ends.

875.691 MPa, respectively. The minimum stress of prestressed tendons in columns were 248.829 and 247.467 MPa for beams (Figure 13). The yield stress is expected to be 1581 and 1673.7 MPa for tendons in columns and beams, respectively. The prestressed tendons were linear elastic in all tests, providing the self-centering capability of the structure after the earthquake.

The rubbers between the column and base were consistently elastic. The yielding strength of the material of angle steel was 235 MPa. The yielding strain is expected to be $1075 \mu\epsilon$. As shown in Table VII, the angle steel was firstly considered yielded during the El Centro 0.20 g test, which resulted in the decrease in frequency after the El Centro 0.20 g test. The strain in the angle steel grew with the increase of PGA. During the test, the maximum strain in the angle steel was $9836 \mu\epsilon$ in the bottom angle steel of beam B1, which was out of order in the second-series test after the peak value state.

4. NUMERICAL SIMULATION

To describe and investigate the seismic behavior of the self-centering structures, a three-dimensional model was created using the software OpenSEES [21] for simulating the nonlinear response under earthquake excitations. Although shear–flexure interaction was not considered, analysis based on fibers was accurate enough to predict both the global and local response of concrete structures [22, 23]. Thus, force-based beam–column elements with fiber sections were used to model the beams and columns. Connection details and simplified models are discussed as follows.

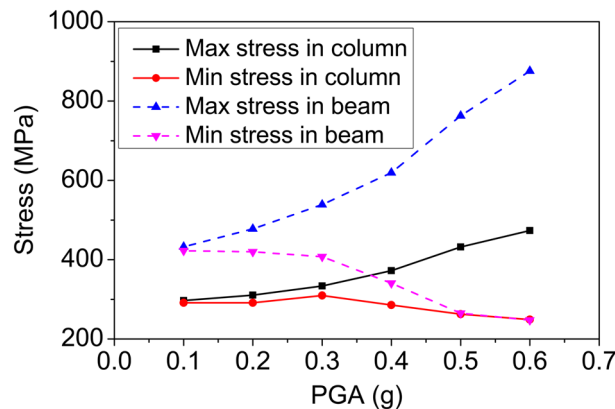


Figure 13. Maximum and minimum stress in prestressed tendons under El Centro NS wave.

4.1. Prestressed tendons

Unbonded PT tendons were modeled by using truss elements along the members (Figure 14). Prestressed duct friction and relaxation resulted in the major loss of prestress. Because of the limitation of truss elements, minor stress difference in tendons caused by column bending was neglected in this study.

To simulate the effect of prestressed tendons, prestress is generally added by lowering the temperature, applying an initial strain or equivalent loading. In this study, initial strain was used to account for the prestress. Taking account of the loss of the stress of the prestressed tendons, which possibly due to the degradation of the system frequencies, different initial strain value was applied to each self-centering beam and column according to the forces of the initial prestress tendons that we got from each sequence of the test. It should be noted that once the initial strain was applied, the beams and columns would be under compression. This would result in a reduction in the axial length and loss in prestress of the tendons after iteration of equilibrium equations. It means that there is a difference between the initial forces, which is caused by the initial strains applied to numerical model, and prestressed forces (showed in Table III), which was measured after prestressing. Clearly, the initial forces are larger than the prestressed forces to provide a more similar condition as the test.

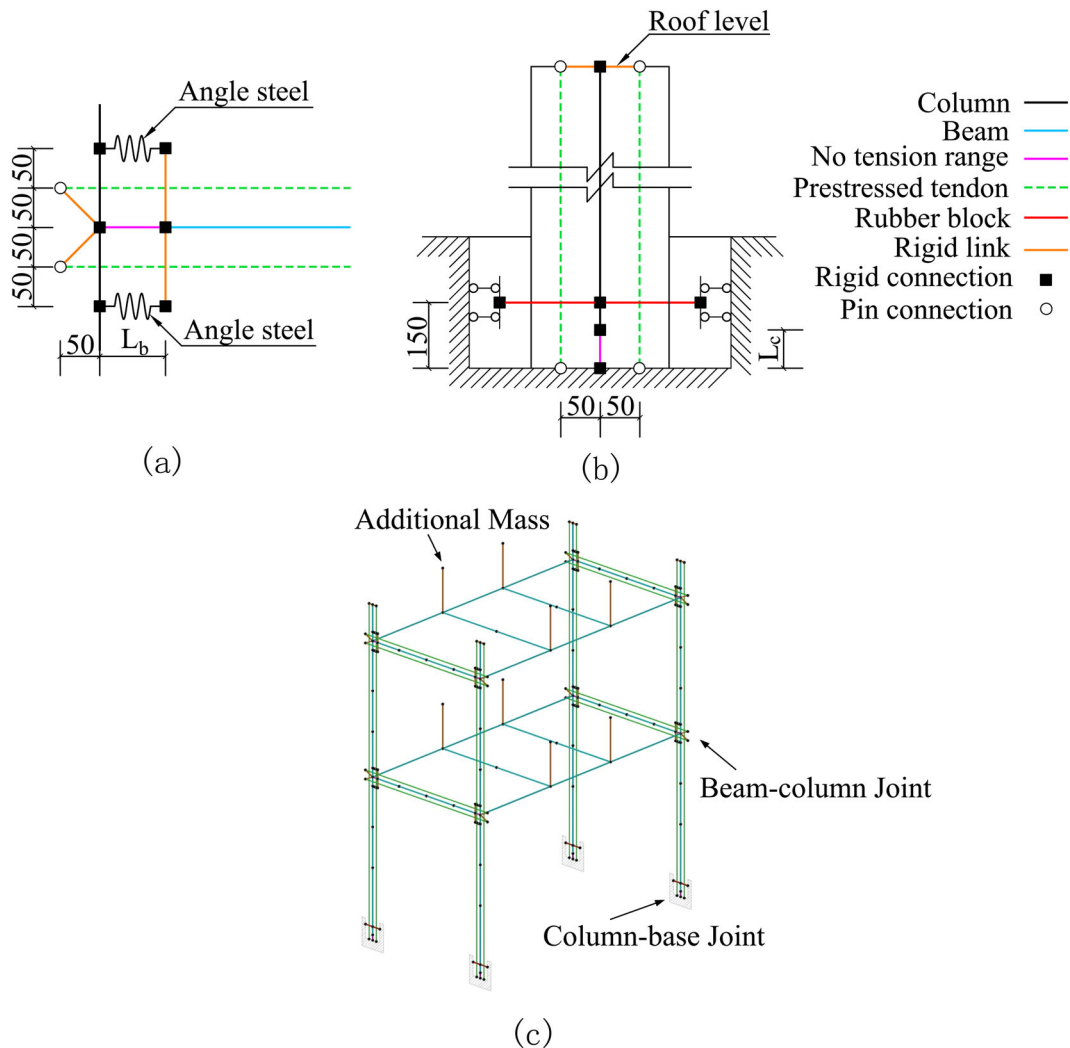


Figure 14. Computational models: (a) beam–column joints, (b) column–base joints, and (c) the structure.

Steel02 material was selected as the constitutive law assigned to truss elements. Although having its own hysteretic rules, *Steel02* should be appropriate for modeling tendons because tendons remained linear elastic over all process according to the design objectives.

Rigid links were used at the end of columns or beams to consider the influence of the column and beam depths, as shown in Figure 14.

4.2. Beam–column connection

Opening at the beam–column interface is an important performance in the behavior of a self-centering connection. It represents the rocking mechanism of the connection. When the stress of the outermost fiber of the section of the beam end equals to zero but the strain of which is not null, the opening is considered to occur, corresponding to the opening mechanism shown in Figure 5(b). Before the opening, the whole section is in compression. Once it occurs, the neutral axis of the section moves into the cross section. Because the beam–column joints have no tension capacity across the interface, nonlinearity of response will develop when the precompression at the extreme compression fiber disappears. The compression zone decreases as the opening increases. Previous studies [24] show that in the simulation of rocking structures, the deformation of compressive zone has to be taken into account for precast reinforced concrete members. Because the contact surfaces could not take any tensile stresses, the ends of the beams were under nonlinear stress distribution. The height of the ‘nonlinear stress zone’ can be obtained by solving the stress distribution near the contact surface. According to the research of Roh *et al.* [25], the actual height of nonlinear stress zone is determined:

$$L_b^* = \frac{1}{2} \sqrt{d^2 - d_c^2 + 2d\sqrt{d^2 - d_c^2}} \quad (1)$$

where d is the column depth and d_c is the contact depth.

For a simplified analytical evaluation, the equivalent height in the linearized system, L_b (Figure 14 (a)), is obtained as

$$L_b = \left(\frac{2}{1+p} \right) L_b^* \quad (2)$$

where p is a degradation parameter that represents the reducing rate of the effective depth from the height of nonlinear stress zone to the contact surface [25].

With the aforementioned in mind, L_b was selected as 70 mm (more details of the formulation are given in Ref. [25]); concrete and reinforcement fibers at the ends of the beams were modeled with no tensile capacity. *Concrete06* material and *Steel02* material were combined with *Elastic-No Tension* material (*ENT* material, Figure 15) separately using *Series material*, to represent the

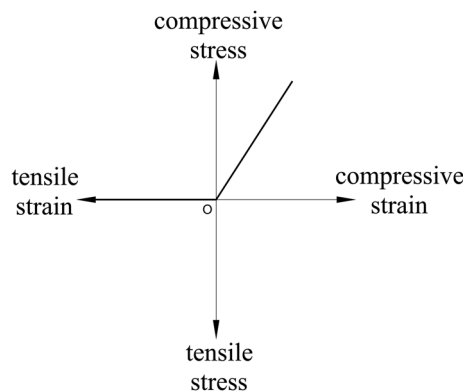


Figure 15. Elastic-no-tension material.

constitutive relations of concrete and reinforcement at the ends of the beams and columns, respectively. The elastic modulus of the *ENT material* must be large enough to eliminate the influence to the compressive stiffness of *Series material*. Enough compressive force was assumed to be provided by prestressed tendons so that angle steel and the friction at the beam–column interfaces transferred the shear force. It also means that the sliding at contact surface between column and beam was not considered in this study.

The complex mechanism of top-and-seat angle steel [26] subjected to seismic forces was simplified by using the behavioral fiber model of Shen *et al.* [27]. This model neglected the effects of prying forces and only the deformation due to flexure and shear in the angle legs were considered. The hysteretic rules of the angle steel model are shown in Figure 16 [27].

Each angle steel in the column–beam connection was modeled as a parallel nonlinear spring, whose force–deformation relationship has been specified in Figure 16, which was implemented in the model using truss elements. As shown in Figure 14(a), one node of the truss element was connected to the column; the other node was connected to the rigid link, which was used to consider the geometric location of angle steel.

4.3. Column–base connection

Rubber blocks between columns and the base were assumed to keep linear elastic in the analysis. Figure 4(b) shows the deformation pattern of rubber blocks when columns rock. Under rocking mechanism, the column will separate from the rubber block at the interface at one side and squeeze the rubber block at the other side. The idealized behavior is illustrated in Figure 17. The mechanism is identical to Euler–Bernoulli beam except that the boundary conditions of the rubber block provide no vertical shear resistance. The *force-based beam–column element* with fiber sections was selected to reflect the property of the rubber blocks described earlier. Fibers of the rubber block were characterized with the compression-only stress–strain relationship using *ENT material*. In addition, the constraint of the translational degree-of-freedom of the nodes at the Z direction (Figure 14) had to be released to model the boundary condition.

The column–base connection has similar characteristics as the beam–column connection. Thus, the same method described in Section 4.2 was adopted to model the column–base connection, except that the range (L_c) of no-tension area was selected as 60 mm (more details of the formulation are given in Ref. [25]). Sliding at the interface between column and base was also neglected.

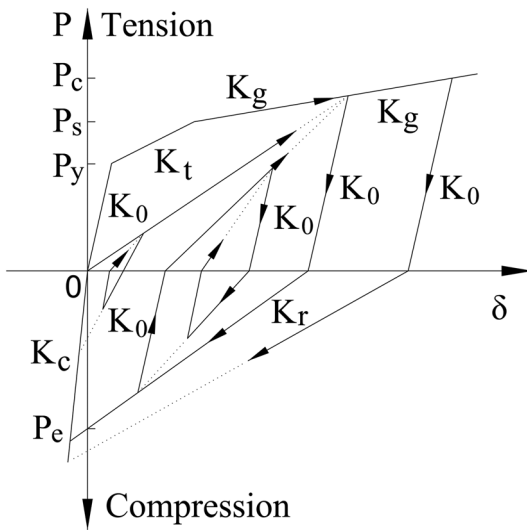


Figure 16. The hysteretic rules of the angle steel model.

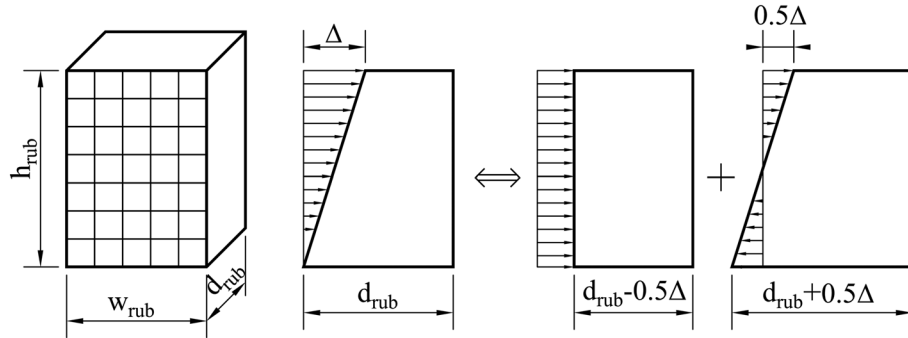


Figure 17. Deformation pattern of rubber blocks.

4.4. Comparison of numerical simulation and experimental results

To verify the proposed numerical methods for evaluating the seismic performance of the tested self-centering reinforcement concrete frame, a series of nonlinear dynamic time history analyses were conducted. The same ground motions used in the experiment were applied to the numerical structural model. Rayleigh damping and a damping ratio of 5% were assigned to the first two modes of the structure. To properly model the structure, stiffness proportional damping was applied only to columns and beams. Components used for connection, such as rigid links, angle steel, rubber blocks, tendons, and the no-tension range of columns and beams, were not included.

The simulation results of global response are illustrated in Table VIII. The results indicated that most of the differences between simulation and test are no more than 10% in the tests. However, with increasing excitation, the difference between simulation and test had an increasing trend. For example, the absolute difference of the maximum relative displacement of the second floor between simulation value and test value under El Centro wave increased from 2.02 to 13.13%. The very likely reason is that when the structure was undergoing large deformation, high geometric nonlinearity occurred, while the numerical model was not able to capture it. The maximum forces of tendons in different cases are shown in Table IX. The table demonstrated that tendons remained in the linear elastic range under all earthquake excitations, which meant the objective of elastic design of prestressed tendons was achieved.

Figure 18 shows the time histories of the displacement at roof level, the forces of tendons, the uplift at the base of the column, and the reaction moment of rubber, respectively. The simulation results presented a sound agreement compared with the test results. Thus, the presented simulation provided a reasonably accurate methodology to analyze the seismic response of the self-centering reinforced concrete frames.

Table VIII. Global response of simulation.

Sequence	Input	PGA (g)	a_{\max} (second floor) (g)			X_{\max} (second floor) (mm)			
			Simu	Test	δ (%)	Simu	Test	δ (%)	
6	El Centro	0.20	0.576	0.649	-11.2	20.201	19.801	2.02	
		0.30	0.781	0.757	3.17	37.585	37.055	1.43	
		0.40	0.986	1.077	-8.45	60.801	64.993	-6.45	
		0.60	1.302	1.455	-10.52	113.876	131.090	-13.13	
		Wenchuan	0.20	0.207	0.206	0.49	12.784	12.708	0.60
			0.30	0.351	0.345	1.74	21.885	21.559	1.51
			0.40	0.421	0.415	1.45	27.011	26.659	1.32
			0.60	0.530	0.562	-5.69	39.061	40.634	-3.87
		0.80	0.587	0.639	-8.14	44.989	47.168	-4.62	

a , acceleration response; X , relative displacement response; Simu, simulation value; Test, test value; δ , difference between the simulation value and test value.

Table IX. Joint response of simulation.

Sequence	Input	PGA (g)	Maximum uplift (mm) (C1)			Maximum opening (mm) (B1)			Force of tendon (kN) (C1L)		
			Simu	Test	δ (%)	Simu	Test	δ (%)	Simu	Test	δ (%)
6	El Centro	0.20	1.183	1.164	1.63	1.308	1.285	1.79	46.0	43.5	5.75
8		0.30	2.218	2.139	3.69	2.466	2.418	1.99	49.7	46.7	6.42
12		0.40	3.724	3.816	-2.41	4.190	4.353	-3.74	54.3	52.1	4.22
17		0.60	7.972	8.123	-1.86	8.988	9.360	-3.97	65.0	66.2	-1.81
20	Wenchuan	0.20	0.654	0.643	1.71	0.812	0.804	1.00	38.8	36.9	5.15
22		0.30	1.165	1.146	1.66	1.417	1.400	1.21	38.9	36.8	5.71
24		0.40	1.335	1.375	-2.91	1.842	1.794	2.68	39.3	36.6	7.38
26		0.60	2.151	2.216	-2.93	2.724	2.812	-3.13	40.1	36.9	8.67
28		0.80	2.391	2.479	-3.55	3.099	3.218	-3.70	44.1	39.3	12.21

B1, beam B1; C1, column C1; L, the left tendon; Simu, simulation value; Test, test value; δ , difference between the simulation value and test value.

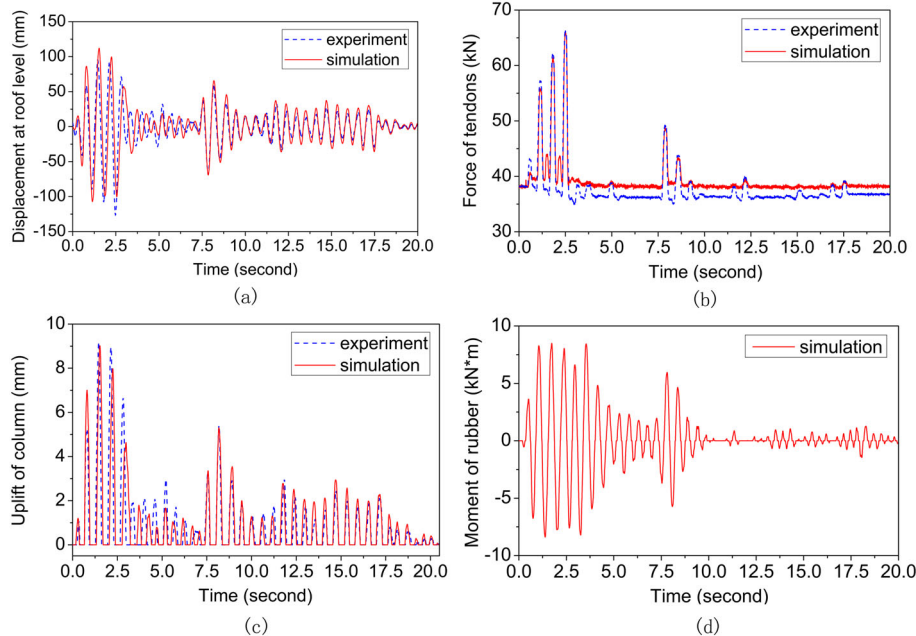


Figure 18. Response time histories of the test frame under El Centro 0.6 g: (a) displacement at roof level, (b) force of tendons, (c) uplift of column, and (d) reaction moment of rubber.

5. CONCLUSIONS

Based on the shaking table test and numerical dynamic analysis of the self-centering reinforced concrete frame, the following conclusions could be drawn:

- (1) The self-centering reinforced concrete frame system has satisfactory seismic performance, under severe earthquakes in particular. The test model stayed elastic under excitation with PGA of 0.20 g. The structure had no severe damage even after it went to 0.60 g.
- (2) The expected self-centering capacity was achieved in the tests. The uplift of columns and opening of beams firstly happened during the El Centro 0.20 g test and the Wenchuan 0.30 g test. After PGA was increased to 0.40 g, the uplift of columns and opening of beams were obviously apparent. Large rocking of structure was obtained under the El Centro 0.60 g test. However, no signal of structural damage appeared. The test model went back to its initial position with negligible residual deformation after the test.

- (3) The major damage happened at the interfaces between angle steel and concrete. No damage was observed on the self-centering elements. The angle steel dissipated energy with large deformation as expected. Yield of angle steel first happened at the El Centro 0.20 g test, which was not a severe excitation. Higher strength of angle steel should be applied to achieve more energy dissipation.
- (4) An OpenSEES-based simulation model was developed to predict the seismic response of the test structure, and the results were verified by the shaking table test. The agreement between them proved that the proposed analytical methodology could also be applied in further studies of self-centering reinforced concrete frames.

This research aims to provide an alternative of traditional seismic force resisting systems with better seismic performance and controllable post-quake repair. To improve the seismic performance of self-centering reinforcement concrete frames, more relative studies are expected, for example, the applications of energy dissipation devices. In the process of validating the simulation model, the following areas are expected for improvements: (1) a more accurate element instead of truss element to model the prestressed tendons; (2) implementing concrete damage model in the numerical analysis; and (3) characterizing the nonlinearity of rubber.

ACKNOWLEDGEMENTS

The financial support of National Nature Science Foundation of China through grant 51261120377 and 91315301-4 is gratefully acknowledged.

REFERENCES

1. Lu XL, Mao YJ, Chen Y, et al. New structural system for earthquake resilient design. *Journal of Earthquake and Tsunami* 2013; **7**(03):1350013-1-26.
2. Zhou Y, Lu XL. State-of-the-art on rocking and self-centering structures. *Journal of Building Structures* 2011; **32**(9): 1–10. (in Chinese)
3. Priestley MJN. Overview of PRESSS research program. *PCI Journal* 1991; **36**(4):50–57.
4. Priestley MJN, Tao JR. Seismic response of precast prestressed concrete frames with partially debonded tendons. *PCI Journal* 1993; **38**(1):58–69.
5. Cheok GS, Lew HS. Model precast concrete beam-to-column connections subject to cyclic loading. *PCI Journal* 1993; **38**(4):80–92.
6. Priestley MJN, Macrae GA. Seismic tests of precast beam-to-column joint subassemblages with unbonded tendons. *PCI Journal* 1996; **41**(1):64–81.
7. Priestley MJN et al. Preliminary results and conclusions from the PRESSS five-story precast concrete test building. *PCI Journal* 1999; **44**(6):42–67.
8. El-Sheikh MT et al. Seismic behavior and design of unbonded post-tensioned precast concrete frames. *PCI Journal* 1999; **44**(3):54–71.
9. Spieth HA, Carr AJ, Murahidy AG, et al. Modelling of post-tensioned precast reinforced concrete frame structures with rocking beam–column connections. *2004 NZSEE Conference*, New Zealand, 2004.
10. Roh H, Reinhorn AM. Nonlinear static analysis of structures with rocking columns. *Journal of Structural Engineering* 2009; **136**(5):532–542.
11. Hawileh RA, Rahman A, Tabatabai H. Nonlinear finite element analysis and modeling of a precast hybrid beam–column connection subjected to cyclic loads. *Applied Mathematical Modelling* 2010; **34**(9):2562–2583.
12. Rojas P, Ricles JM, Sause R. Seismic performance of post-tensioned steel moment resisting frames with friction devices. *Journal of Structural Engineering* 2005; **131**(4):529–540.
13. Garlock MM, Sause R, Ricles JM. Behavior and design of posttensioned steel frame systems. *Journal of Structural Engineering* 2007; **133**(3):389–399.
14. Midorikawa M, Ishihara T, Azuhata T, et al. Three-dimensional shaking table tests on seismic response of reduced-scale steel rocking frames. *Proceedings of the 3rd International Conference on Advances in Experimental Structural Engineering*, San Francisco, USA, 2009.
15. Ma X, Deierlein G, Eatherton M, et al. Large-scale shaking table tests of steel braced frame with controlled rocking and energy dissipating fuses. *Proceedings of the 9th US National and 10th Canadian Conference on Earthquake Engineering*, Toronto, Canada, 2010.
16. Ministry of Housing and Urban–Rural Development of the People’s Republic of China. *GB 50010-2010 Code for Design of Concrete Structures*. Architecture & Building Press: Beijing, China, 2010. (English version)
17. Lu XL, Fu GK, Shi WX, et al. Shake table model testing and its application. *Struct. Design Tall Spec. Build.* 2008; **17**:181–201.
18. New Zealand Standards (NZS). *NZS 3101:2006, Concrete Design Standard*. The Colour Guy: Wellington, New Zealand, 2006.

19. Yuan RW, *et al.* Calculation of initial stiffness and ultimate bearing capacity of top-and-seat angle connections. *Building Structure* 2009; **39**(9): 91–93. (in Chinese)
20. Ministry of Housing and Urban-Rural Development of the People's Republic of China. *GB 50011-2010 Code for Seismic Design of Buildings*. Architecture & Building Press: Beijing, China, 2010. (English version)
21. McKenna F, Fenves GL, Scott MH, Jeremic B. *Open System for Earthquake Engineering Simulation (OpenSEES) [Software]*. Pacific Earthquake Engineering Research Center, University of California: Berkeley, CA, 2013.
22. Spaccone E, Filippou FC, Taucer FF. Fibre beam–column model for non-linear analysis of R/C frames: Part II. Applications. *Earthquake Engineering and Structural Dynamics* 1996; **25**(7):727–742.
23. Mayer U, Eligehausen R. Bond behavior of ribbed bars at inelastic steel strains. *Proceedings of 2nd International Ph. D. Symposium in Civil Engineering*, Technical University of Budapest, Hungary, 1998: 39–46.
24. Pampanin S, Priestley MJN, Sritharan S. Analytical modeling of the seismic behaviour of precast concrete frames designed with ductile connections. *Journal of Earthquake Engineering* 2001; **5**(03):329–367.
25. Roh H, Reinhorn AM. Analytical modeling of rocking elements. *Engineering Structures* 2009; **31**(5):1179–1189.
26. Garlock MM, Ricles JM, Sause R. Cyclic load tests and analysis of bolted top-and-seat angle connections. *Journal of Structural Engineering* 2003; **129**(12):1615–1625.
27. Shen J, Astaneh-Asl A. Hysteresis model of bolted-angle connections. *Journal of Constructional Steel Research* 2000; **54**(3):317–343.